Concentration of crustal displacement along a weak Altyn Tagh fault: Evidence from paleomagnetism of the northern Tibetan Plateau

Guillaume Dupont-Nivet, Delores Robinson, Robert Butler, An Yin, H. Jay Melosh

Concentration of crustal displacement along a weak Altyn Tagh fault: Evidence from paleomagnetism of the northern Tibetan Plateau

Guillaume Dupont-Nivet,[1] Delores Robinson,[2] and Robert F. Butler

Department of Geosciences, University of Arizona, Tucson, Arizona, USA

An Yin

Department of Earth and Space Sciences, University of California, Los Angeles, California, USA

H. Jay Melosh

Department of Geosciences, University of Arizona, Tucson, Arizona, USA

Received 11 April 2002; accepted 11 November 2003; published 27 February 2004.

[1] Like many regional structures in the northern Tibetan Plateau, the Tula syncline changes strike by ~40° from NW-SE to nearly EW as it approaches the Altyn Tagh fault from the south. To test whether this strike curvature is due to oroclinal bending, we analyzed paleomagnetic samples from 109 sites collected from Late Jurassic to Paleogene red sedimentary strata of the Tula syncline. Fold and reversal tests suggest a primary origin for the characteristic remanent magnetization from nine sites in the eastern half and 41 sites in the western half of the syncline. The observed 13.3°±8.8° declination difference between the two halves of the Tula syncline is far less than the ~40° difference predicted for oroclinal bending. Instead the arc shape of the syncline is an original configuration produced by transport above an arcuate thrust ramp. Along with paleomagnetic data from the northern Qaidam Basin, these results from the Tula syncline indicate that crustal displacement between the Tarim Basin and the northern Tibetan Plateau is accommodated by strike-slip motion on the Altyn Tagh fault rather than distributed shear within the northern Tibetan Plateau. *INDEX TERMS:* 1525 Geomagnetism and Paleomagnetism: Paleomagnetism applied to tectonics (regional, global); 1527 Geomagnetism and Paleomagnetism: Paleomagnetism applied to geologic processes; 8102 Tectonophysics: Continental contractional orogenic belts; 8164 Tectonophysics: Stresses—crust and lithosphere; 8010 Structural Geology: Fractures and faults; *KEYWORDS:* Altyn Tagh fault, central Asia, paleomagnetism, strike-slip systems, oroclinal bending. **Citation:** Dupont-Nivet, G., D. Robinson, R. F. Butler, A. Yin, and H. J. Melosh (2004), Concentration of crustal displacement along a weak Altyn Tagh fault: Evidence from paleomagnetism of the northern Tibetan Plateau, *Tectonics*, *23*, TC1020, doi:10.1029/2002TC001397.

1. Introduction

[2] The Altyn Tagh fault (ATF), the most prominent strike-slip fault in Asia (Figure 1), plays a key role in accommodating Indo-Asian continental collision [*Molnar and Tapponnier*, 1975]. One view is that deformation of the Tibetan Plateau is concentrated on major faults bounding quasi-rigid blocks [*Tapponnier et al.*, 1982]. In this model, left slip on the ATF transfers a significant portion of the convergence between India and Asia into northeastward extrusion of the Tibetan Plateau. An alternative view is that continental lithosphere behaves as a viscous fluid with deformation more broadly distributed [*England and McKenzie*, 1982; *Houseman and England*, 1996]. An important aspect of the ATF is the conversion of strike-slip motion on the south side of the fault into thrust faulting and crustal thickening at its eastern terminus [*Burchfiel et al.*, 1989; *Yin and Nie*, 1996]. This process is believed to result in eastward growth of the northern boundary of the Tibetan Plateau [*Meyer et al.*, 1998].

[3] Many thrust faults of the northern Tibetan Plateau (e.g., Qimen Tagh thrust, Figure 1) curve from WNW-ESE strike far south of the ATF to nearly E-W orientation close to the fault. An obvious question is whether the present curvature of these thrust faults is an original geometry or instead resulted from oroclinal bending of thrust faults that were originally straight (Figure 2 [*Yin and Harrison*, 2000; *Yue et al.*, 2001]. The answer to this question has tectonic significance because of the implied concentrated or distributed nature of crustal displacement between the Tarim Basin and the northern Tibetan Plateau. If this displacement is concentrated along the ATF, then piercing point offsets provide a measure of the total displacement between the Tarim Basin and the Tibetan Plateau. If deformation is

[1]Now at Paleomagnetic Laboratory "Fort Hoofddjk," Utrecht University, Utrecht, Netherlands.

[2]Now at Department of Geological Sciences, University of Alabama, Tuscaloosa, Alabama, USA.

0278-7407/04/2002TC001397$12.00

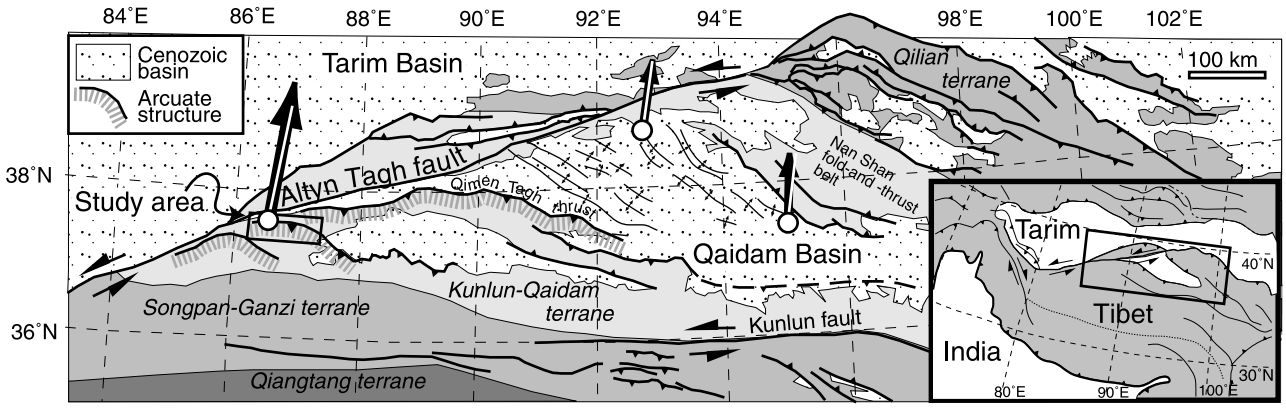

Figure 1. Map of eastern Altyn Tagh fault and adjacent regions with tectonostratigraphic terranes (shades of gray), basins, and major faults after *Yin and Harrison* [2000]. Inset at lower right shows regional location. Most prominent arcuate structures are illustrated. Box labeled "study area" is illustrated in Figure 3. Large arrow is observed paleomagnetic declination from this study compared to expected declination shown by white line. Smaller arrows are paleomagnetic declinations observed from Qaidam Basin compared with expected declinations shown by white lines [*Dupont-Nivet et al.*, 2002a]. For a review of paleomagnetic declination results in the Altyn Tagh Fault region, see *Dupont-Nivet et al.* [2003].

distributed south of the ATF into the northern Tibetan Plateau, then offset along the ATF is less than the total Tarim Basin-Tibetan Plateau displacement; the additional amount of distributed deformation within the northern Plateau would have to be determined to infer the total displacement between the Tarim Basin and the Tibetan Plateau. We used paleomagnetic declinations observed along an arcuate structure south of Tula to test whether its curvature resulted from oroclinal bending in a drag-fold fashion or instead originally developed as a curved structure (Figures 2 and 3).

2. Geologic Setting

[4] Geologic mapping of the Tula arcuate syncline and surrounding areas indicates that the controlling structures are northeast vergent thrust faults (Figure 3) [*Robinson et al.*, 2002]. The structurally higher thrust fault is a basement-cored uplift with continental Late Jurassic to Early Tertiary red sedimentary strata in the footwall. The structurally lower fault to the east thrusts these red beds onto Quaternary gravels (Figure 3). These red sedimentary rocks constituting the main target of paleomagnetic sampling are deformed into a broad footwall syncline (henceforth referred to as the Tula syncline) that changes strike by $\sim$40° from WNW-ESE to nearly E-W as it approaches the ATF from the south.

[5] Three main units are described in the red sedimentary strata. The lower unit is thick green conglomerate beds with intercalated red siltstones grading into variegated fine sandstone to mudstone. A Late Jurassic age is assigned to this unit [*Guo et al.*, 1998]. The middle unit is mainly fine sandstone with intercalated conglomerate. A Cretaceous age is indicated by stratigraphic correlation [*Xinjiang Bureau of Geological and Mineral Resources* (*XBGRM*), 1993], while trydactil vertebrate tracks found in this unit were used to assign a Paleogene age [*Lockley et al.*, 1999]. *Robinson et al.* [2002] have confirmed the Cretaceous age by U/Pb dating of an intruding granitic body yielding a minimum age of circa 74 Ma. The conglomerate strata forming the highest unit are assigned a Paleogene age based on fossil assemblages in regionally correlated stratigraphic formations [*XBGRM*, 1993].

3. Paleomagnetic Sampling and Analysis

[6] Sampling was done during two field seasons. An initial "distributed" sampling of 64 sites ($\geq$8 samples per site with 1 sample per stratigraphic level) was designed to obtain samples from the entire area and from a variety of lithologies within the exposed formations. Results from this sampling indicated which rock types provided the most

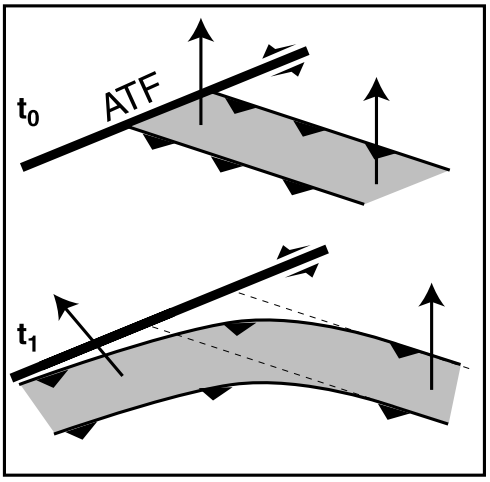

Figure 2. A counterclockwise deflection of paleomagnetic declinations (arrows) is expected for the oroclinal-bending hypothesis.

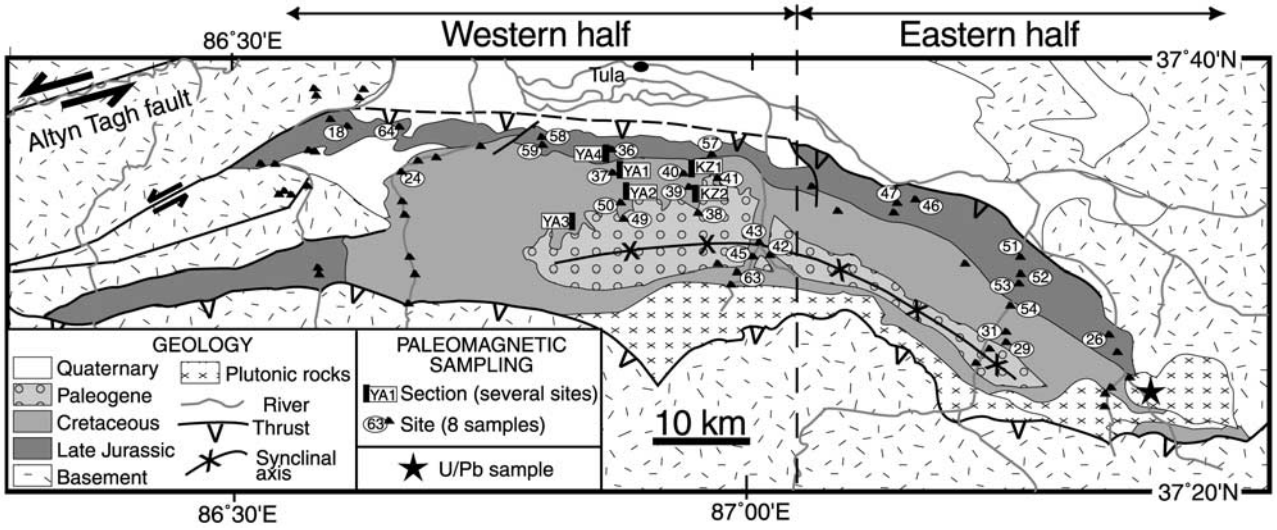

Figure 3. Simplified geologic map of the Tula syncline area showing locations of the sampling sites and sections. Site number is indicated only for sites yielding interpretable results.

reliable paleomagnetic directions and where tectonic rotations were most likely to have occurred. During the second "intensive" sampling, 45 sites ($\geq$8 samples per site = stratigraphic level) were collected from the western portion of the structure in four sections in the Yaousere Valley (28 sites labeled YA) and two sections in the Kezele Valley (17 sites labeled KZ). Bedding attitudes were measured at each sampling site and were also constrained by the geologic mapping. Plunge of the synclinal axis was less than 6° at all sites except JO26 at the eastern end of the syncline with plunge of 21°. Only for this latter site was a plunge correction applied.

[7] All samples were stored, thermally demagnetized and measured in a magnetically shielded room with average field intensity below 200 nT. Measurements of natural remanent magnetization (NRM) were done using a three-axis cryogenic magnetometer (2G model 755R). Following initial NRM measurements, samples were thermally demagnetized in 10 to 20 steps from 50 to 700°C with increments as small as 5°C. When vector end points showed a trend toward the origin of orthogonal projection diagrams, principal component analysis of NRM at $\geq$ four successive temperature steps was used to determine the characteristic remanent magnetization (ChRM) [*Kirschvink*, 1980]. ChRM directions with maximum angular deviation (MAD) greater than 15° were rejected from further analysis (Figure 4). Following determination of ChRM directions from $\geq$ four samples from a site, site-mean ChRM directions were calculated using statistical methods of *Fisher* [1953]; sample ChRM directions more than two angular standard deviations from the preliminary site-mean direction were rejected prior to calculation of the final site-mean direction. Site-mean ChRM directions with 95% confidence interval (α_{95}) greater than 25° were rejected for further

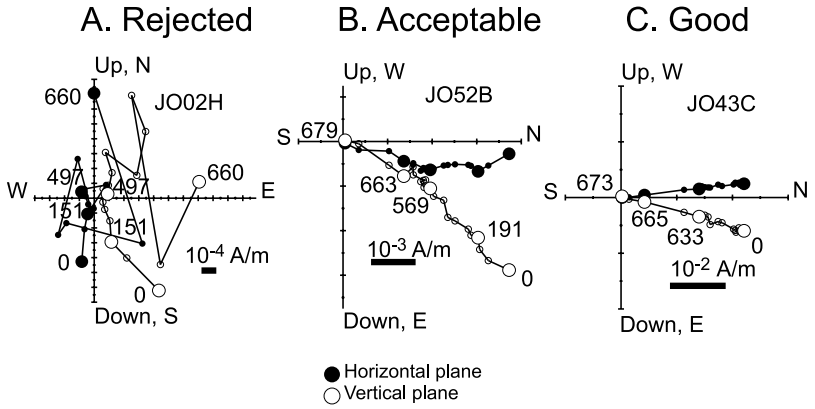

Figure 4. Vector-component diagrams of thermal demagnetization behavior. (a) Sample JO02H from which no ChRM direction could be determined. (b and c) Samples JO52B and JO43C yielding interpretable ChRM directions. Open circles are projections onto vertical plane and filled circles are projections onto horizontal plane. Numbers adjacent to data points indicate temperature in °C.

analysis. Using the same methods, mean paleomagnetic directions were calculated for separate sampled sections and for different parts of the Tula syncline.

[8] During the Late Jurassic to Early Tertiary age interval of the sampled formations, the Apparent Polar Wander Path (APWP) for Asia makes a "hairpin loop" [*Enkin et al.*, 1991]. This permits direct comparison of paleomagnetic directions from rocks of different ages to determine relative vertical-axis tectonic rotations. Also vertical-axis rotations with respect to "stable" Asia can be accomplished by comparing observed paleomagnetic directions with expected directions computed from the averaged paleomagnetic pole position (latitude, 79.8°N; longitude, 190.2°E; A_{95}: 2.3° [*Besse and Courtillot*, 2002]. Confidence limits on vertical-axis rotations were determined using the procedures of [*Demarest*, 1983]. An additional benefit of the hairpin in the APWP is that uncertainties in age of the sampled rocks have little effect on the inferred vertical-axis rotations.

3.1. Distributed Sampling

[9] Out of the 64 sites in the initial distributed sampling, results from pilot samples from ten sites in various sedimentary, plutonic, and volcanic rocks could not be interpreted due to poor structural control and/or very low NRM intensity. Samples from the remaining 54 sites in red sedimentary strata were thermally demagnetized. Site-mean ChRM directions could not be determined for 27 sites due to failure of the criteria outlined above. Samples from these sites generally had low NRM intensity ($<5 \times 10^{-4}$ A/m), unblocking temperatures below 500°C, and erratic demagnetization behaviors. At these rejected sites, visible calcite was noted in outcrop as well as during microscopic examination of thin sections. Many of these sites were collected from deformed rocks near major faults and from coarse-grained and light-colored sandstones. We attribute these properties to chemical alteration by fluid circulation. Thermal demagnetization of samples from the remaining 27 sites revealed a ChRM component isolated at high unblocking temperatures (typically 640 to 675°C) suggesting that hematite is the NRM carrier. The average MAD for the ChRM component determined by principal component analysis was 6.9° and examples of demagnetization behaviors are illustrated in Figure 4. Site-mean ChRM directions are listed in Table 1 and two sites with α_{95} greater than 25° were rejected from further analysis.

3.2. Intensive Sampling

[10] Although coarse-grained and visibly deformed sandstones were avoided, samples from 17 out of the 45 sites from the intensive sampling showed erratic behavior and low NRM intensity. These sites were collected in fine-grained layers that often displayed calcite-cemented joints probably resulting from fracturing and fluid circulation concentrated in these beds. For the remaining sites, thermal demagnetization of higher intensity NRM (typically above 5×10^{-3} A/m) yielded ChRM components with unblocking temperatures commonly in the 640 to 675°C range suggesting the NRM is carried by hematite. An average of 7.3° was observed for the MAD calculated during principal component analysis. Two sites yielding only three sample ChRM directions (other samples destroyed during sample preparation) were rejected. Site-mean directions for 11 sites from the Kezele Valley and 15 sites from the Yaousere Valley are listed in Table 1; one site-mean direction with α_{95} greater than 25° was rejected from further analysis.

3.3. Field Tests of Paleomagnetic Stability

[11] To test for oroclinal bending of the Tula syncline, we must compare paleomagnetic directions between the two halves of the structure with different trends. The western half of the syncline trends N85°E, while the eastern half trends S55°E (Figure 3). Following this change in trend, we divide the paleomagnetic sites into "western sites" (41 sites) and "eastern sites" (9 sites) as indicated in Table 1. Field tests of paleomagnetic stability are applied separately to data from the western sites and data from the eastern sites prior to comparing mean paleomagnetic directions between the western and eastern halves of the syncline.

[12] For both the western and eastern areas, site-mean paleomagnetic directions cluster in antipodal normal and reverse polarity directions (Figure 5). The eastern sites pass the fold test of [*McFadden*, 1990] at 99% confidence (in situ statistics: $\xi = 5.667$ and $k = 19.1$; tilt-corrected statistics: $\xi = 0.027$ and $k = 39.1$; $\xi = 4.849$ is 99% confidence limit for $N = 9$). However, the reversal test of [*McFadden and McElhinny*, 1990] is indeterminate, probably because there are only two reverse polarity sites. Nevertheless, after tilt correction, the antipode of the mean reverse polarity direction is indistinguishable from the mean normal polarity direction.

[13] The western sites pass the reversal test [*McFadden and McElhinny*, 1990] with C classification (angle between normal polarity mean and antipode of reverse polarity mean = 2.1°; critical angle = 11.8°). The western sites collected during the second field season were from five homoclinal stratigraphic sections, each with a single average tilt correction. We applied the fold test to the five section-mean directions (given in Table 1) and the 16 site-mean directions from the distributed sampling that have independent tilt corrections. Using the procedure of [*McFadden*, 1990], the western sites pass the fold test at 99% confidence (in situ statistics: $\xi = 8.97$ and $k = 6.62$; tilt-corrected statistics: $\xi = 0.739$ and $k = 20.54$; $\xi = 7.483$ is 99% confidence limit for $N = 21$).

4. Discussion and Conclusions

[14] When comparing the paleomagnetic directions between the two halves of the Tula syncline, the immediately apparent result is that the observed difference in declinations (13.3° ± 8.8°) is far less than the ~40° declination difference predicted for oroclinal bending (Figures 2 and 5). The main conclusion of this study is that the ~40° bend of the Tula syncline is not due to oroclinal bending by distributed deformation of the northern Tibetan Plateau. Instead the arcuate shape of the Tula syncline is largely or entirely the original configuration of this structure. Furthermore, comparison of the observed mean paleomagnetic declina-

Table 1. Site-Mean Directions[a]

				In Situ		Tilt Corrected						
Sites	Fm.	Lat., °N	Long., °E	*I*, deg	*D*, deg	*I*, deg	*D*, deg	α_{95}, deg	*k*	*n*/*N*	Dip, deg	Dip az., deg
						Eastern Sites						
JO26	J	37.455	87.351	−28.0	191.4	−8.0	199.3	19.3	8.0	8/8	24.8	226.1
JO29	K	37.450	87.239	30.6	20.5	40.4	5.4	14.3	23.8	5/7	22.9	258.1
JO31	K	37.459	87.248	13.9	25.0	42.4	21.5	24.1	6.2	7/7	29.2	215.9
JO46	J	37.560	87.160	14.3	19.7	46.9	31.0	13.1	14.6	9/9	37.1	175.6
JO47	J	37.560	87.143	0.5	30.2	26.9	31.9	19.4	9.1	7/7	27.2	196.5
JO51	J	37.521	87.261	3.2	26.8	37.1	26.3	13.3	18.5	7/8	33.9	208.9
JO52	J	37.501	87.262	22.0	32.4	42.5	19.7	10.6	28.7	7/8	28.2	250.3
JO53	J	37.496	87.260	34.4	14.4	37.9	5.5	13.9	17.0	7/7	12.6	263.9
JO54	K	37.478	87.249	20.2	209.4	−21.6	209.3	18.5	10.0	7/7	42.3	219.0
Mean East		37.498	87.241	14.3	23.6			12.1	19.1	9/9		
Mean East		37.498	87.241			34.2	21.3	9.6	29.7	9/9		
						Western Sites						
JO18	J	37.619	86.605	6.7	198.9	−42.8	205.1	16.6	12.2	7/7	52.2	182.1
JO24	K	37.580	86.660	38.6	35.9	51.2	20.7	21.1	7.8	6/6	31.5	99.9
JO36	J	37.604	86.844	1.5	158.7	−25.4	159.2	11.2	25.9	7/7	27.0	153.8
JO37	K	37.579	86.864	−23.1	9.6	24.4	9.7	19.7	7.8	8/8	48.8	175.6
JO38[b]	K	37.554	86.945	−39.7	188.3	−25.9	192.5	27.4	5.0	7/7	15.7	216.2
JO39	K	37.571	86.937	4.8	186.9	−25.1	186.9	18.6	14.3	5/5	29.9	187.0
JO40	K	37.579	86.936	23.4	161.1	−18.5	161.9	21.2	11.2	5/6	45.2	184.7
JO41	K	37.575	86.964	−4.7	352.5	34.6	348.4	23.2	9.5	5/7	41.8	191.2
JO42	K	37.517	87.019	−36.7	212.2	−20.9	204.5	20.8	8.1	7/7	20.9	346.9
JO43	K	37.533	87.009	4.9	24.2	19.6	23.1	15.1	12.6	8/8	15.5	222.7
JO45	K	37.511	86.999	−61.4	262.8	−36.2	205.6	21.0	9.3	6/6	49.6	349.3
JO49	P	37.542	86.876	23.9	16.0	41.4	21.8	21.1	7.8	7/7	19.6	171.5
JO50[b]	K	37.553	86.871	9.8	164.9	11.9	164.0	24.8	6.9	6/6	22.6	176.3
JO57	J	37.594	86.961	−12.1	355.3	36.5	353.8	15.7	16.0	6/6	49.0	182.1
JO58	J	37.609	86.795	−0.5	176.9	−27.5	173.5	17.4	9.7	8/8	30.0	201.8
JO59	J	37.602	86.794	14.2	202.9	−26.8	203.2	20.0	8.6	7/7	41.1	199.2
JO63	K	37.507	86.987	−60.7	190.6	−20.8	190.3	13.6	34.9	4/5	39.9	9.9
JO64	J	37.599	86.670	−4.9	172.1	−33.0	170.3	24.5	8.5	5/6	28.5	181.6
YA1-01	K	37.579	86.864	−27.7	30.2	13.1	26.7	6.0	103.5	7/7	47.7	175.7
YA1-02	K	37.579	86.864	−29.6	28.2	12.1	24.3	9.7	33.9	8/8	47.7	175.7
YA1-03	K	37.579	86.864	−36.7	7.4	10.3	5.2	8.2	46.2	8/8	47.7	175.7
YA1-04	K	37.579	86.864	0.9	1.5	48.3	4.4	19.8	10.2	7/7	47.7	175.7
YA1-05	K	37.579	86.864	−44.0	346.9	3.3	349.3	12.6	24.0	7/7	47.7	175.7
YA1-06	K	37.579	86.864	−7.2	355.5	40.5	355.4	23.2	11.9	5/5	47.7	175.7
YA1-07	K	37.579	86.864	−15.8	340.0	30.1	338.2	20.1	12.1	6/6	47.7	175.7
YA1-08	K	37.579	86.864	−4.3	19.0	38.9	26.1	11.3	29.7	7/7	47.7	175.7
YA2-09	K	37.577	86.865	30.8	172.3	−9.8	174.2	10.7	39.8	6/6	41.6	187.0
YA2-11[b]	K	37.577	86.865	10.9	187.1	−30.7	187.1	38.3	6.7	4/4	41.6	187.0
YA3-13	K	37.551	86.849	−3.3	203.4	−21.6	206.3	15.0	38.7	4/4	22.3	169.5
YA3-14	K	37.551	86.849	−15.8	199.1	−34.7	204.8	11.1	30.4	7/7	22.3	169.5
YA3-15	K	37.551	86.849	4.1	191.2	−16.6	192.1	7.0	62.8	8/8	22.3	169.5
YA3-16	K	37.551	86.849	−8.3	186.1	−29.5	188.5	14.0	30.6	5/5	22.3	169.5
YA3-17	K	37.551	86.849	−0.1	181.0	−21.9	181.9	7.6	63.7	7/7	22.3	169.5
KZ1-02	K	37.579	86.936	5.4	198.3	−35.8	199.2	23.8	11.3	5/5	41.3	194.4
KZ1-04	K	37.579	86.936	15.2	176.0	−24.0	175.0	6.4	76.3	8/8	41.3	194.4
KZ1-05	K	37.579	86.936	16.8	178.0	−22.9	177.4	6.3	93.9	7/7	41.3	194.4
KZ1-06	K	37.579	86.936	22.1	177.2	−17.6	177.7	4.9	189.8	6/6	41.3	194.4
KZ1-07	K	37.579	86.936	30.8	171.5	−7.9	174.6	17.8	19.5	5/5	41.3	194.4
KZ1-08	K	37.579	86.936	4.5	189.5	−36.6	188.2	15.9	24.2	5/5	41.3	194.4
KZ2-10	K	37.571	86.937	−22.8	212.4	−53.0	224.9	5.0	93.6	10/10	33.6	191.2
KZ2-11	K	37.571	86.937	22.0	220.7	−7.7	218.7	11.8	33.3	6/6	33.6	191.2
KZ2-15	K	37.571	86.937	−3.9	187.1	−37.4	186.1	14.3	18.9	7/7	33.6	191.2
KZ2-16	K	37.571	86.937	−17.5	172.1	−48.5	163.1	19.6	8.9	8/8	33.6	191.2
KZ2-17	K	37.571	86.937	7.3	211.8	−24.0	213.7	17.1	21.0	5/5	33.6	191.2
Mean West		37.570	86.885	−3.5	8.8			8.4	8.0	41/44		
Mean West		37.570	86.885			28.6	8.3	5.5	17.5	41/44		
						Western Sections						
Mean YA1	K	37.579	86.864	−21.4	6.2	25.6	6.5	16.7	12.0	8/8	47.7	175.7
Mean YA2	K	37.577	86.865	−30.8	−7.7	9.8	−5.8	10.7	39.8	1/1	41.6	187.0
Mean YA3	K	37.551	86.849	4.7	12.1	25.1	14.6	11.4	46.2	5/5	22.3	169.5
Mean KZ1	K	37.579	86.936	−16.0	2.1	24.4	1.4	11.6	34.0	6/6	41.3	194.4
Mean KZ2	K	37.571	86.937	3.2	20.8	36.2	23.1	26.8	9.1	5/5	33.6	191.2

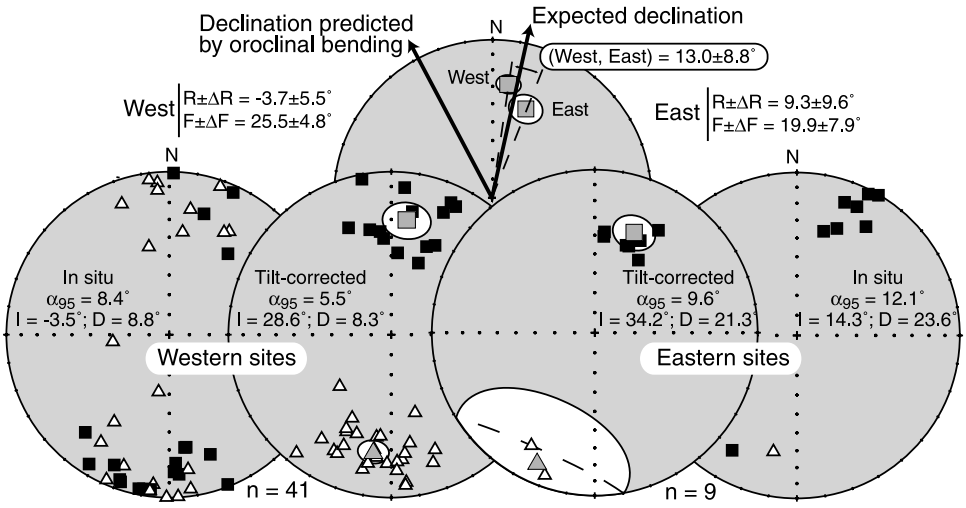

Figure 5. Equal-area projections showing paleomagnetic directions. Bottom diagrams compare in situ and tilt-corrected site-mean ChRM directions for western and eastern halves of the Tula syncline. Black squares indicate directions in lower hemisphere; white triangles indicate directions in upper hemisphere. In tilt-corrected coordinates, larger gray symbols with 95% confidence ellipse are mean of normal polarity directions compared to the mean of reverse polarity directions. Mean declination (D) and inclination (I) with confidence limit (α_{95}) and number of sites (n) are listed for each case. Upper diagram compares tilt-corrected mean directions from eastern and western halves of the Tula syncline. R ± ΔR and F ± ΔF are rotation and flattening with 95% confidence interval derived from observed mean directions minus expected direction calculated from the composite pole for Eurasia [*Besse and Courtillot*, 2002]. Observed flattening is interpreted to result from a rock magnetic effect during compaction and/or deposition processes as discussed by *Dupont-Nivet et al.* [2002a, 2002b].

tions from the Tula syncline with the expected declination computed from the Eurasian reference pole indicates the eastern half is rotated clockwise 9.3° ± 9.6° and the western portion is rotated counterclockwise 3.7° ± 5.5° (Figure 5). Neither rotation with respect to the expected declination is significant at 95% confidence, although the clockwise deflection for the eastern half is nearly so. Although our first-order conclusion is that the large (∼40°) bend of the Tula syncline in map view is not the result of oroclinal bending, the small (13.3° ± 8.8°) difference in paleomagnetic declinations between the two halves of this structure may still be tectonically significant. We speculate that the small clockwise deflection of the eastern half of the Tula syncline is due to transport above an arcuate thrust ramp (Figure 6a). The three-dimensional form of this arcuate thrust ramp is approximately that of a right-stepping oblique ramp with 40° angle between the strike of the oblique ramp and the transport direction (Figure 6b). Analytical and experimental models of deformation within thrust sheets above oblique thrust ramps have been examined by *Apotria et al.* [1992] and *Wilkerson et al.* [1992], respectively. Although modeled deflections of thrust sheets above oblique ramps depend on ramp cutoff angle and details of the analytical method, predicted deflections are uniformly clockwise and range from ∼6° to ∼26° bracketing the observed 13.3°±8.8° clockwise deflection of the eastern half of the Tula syncline relative to the western half of the structure (Figure 6b).

[15] Similar non-rotated paleomagnetic declinations have been observed in Tertiary sediments in the vicinity of the ATF including the northern Qaidam Basin (Figure 1 [*Dupont-Nivet et al.*, 2002a]), the Nan Shan fold-thrust belt and the Altyn Tagh range (see compilation of paleomagnetic declinations given by *Dupont-Nivet et al.* [2003]). If shear was distributed away from the fault, systematic counterclockwise rotations increasing with proximity to the fault would be expected [*England and Wells*, 1991; *McKenzie and Jackson*, 1983; *Nelson and Jones*, 1987]. The lack of such rotations along the entire length of the ATF thus indicates that crustal displacements are concentrated on the fault itself with little or no distributed sinistral shear. The major implication of this result is that the ATF is weak relative to the strength of

Notes to Table 1.

[a]Definitions are as follows: Sites, site identification; Fm., sampled formation (J, Late Jurassic; K, Cretaceous; P, Paleogene); Lat., Long., latitude and longitude of sampling locality; in situ and tilt corrected site-mean paleomagnetic directions given by I, inclination and D, declination; α_{95}, radius of 95% confidence circle of mean direction; k, concentration parameter; n/N, n, number of ChRM directions considered for the mean direction calculation, N, total number of ChRM directions; dip and dip az., mean dip and dip azimuth of bedding attitude. Eastern sites, site-mean results from the eastern portion. Western sites, site-mean results from the western portion. Western sections, section-mean results from western portion.

[b]Discarded site.

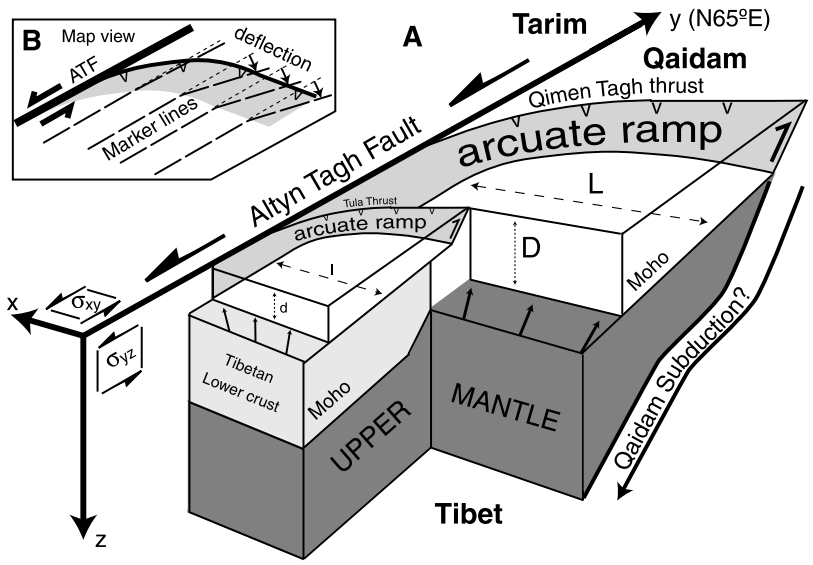

Figure 6. (a) Block diagram showing arcuate structures of different scales branching from the left-lateral Altyn Tagh fault (ATF). See Appendix A for definition of x, y, z, σ_{xy}, σ_{zy}, d, D, l and L. Expected compressional direction rotating with proximity to weak ATF are shown by arrows. (b) Map view showing predicted marker line deflection as thrust sheet passes over an oblique thrust ramp [*Apotria et al.*, 1992; *Wilkerson et al.*, 1992].

surrounding blocks; a key requirement for extrusion tectonics with rigid crustal blocks and strain concentrated on major faults [*Avouac and Tapponnier*, 1993; *Peltzer and Saucier*, 1996; *Tapponnier et al.*, 1982]. A corollary of that implication is that strike-slip offset of geologic piercing points across the ATF account for most or all of the displacement between the Tarim Basin and the northern Tibetan Plateau such that contrasting interpretations of Quaternary slip rate along the ATF are probably not the result of strike-slip strain distributed outside the areas examined in those studies [*Bendick et al.*, 2000; *Burchfiel et al.*, 1989; *Meriaux et al.*, 2000; *Meyer et al.*, 1998; *Molnar et al.*, 1987; *Peltzer et al.*, 1989; *Washburn et al.*, 2003].

[16] A remaining question is the mechanism by which arc-shaped thrust faults south of the ATF are formed. Similar to the San Andreas fault system of central California, the weakness of the ATF implied by our paleomagnetic data requires a reorientation of far field stresses in the vicinity of the fault trace [*Zoback*, 2000; *Zoback et al.*, 1987]. Shear stresses that are constrained by the frictional strength of the rock away from the fault are not sustained near the weak ATF. The expected swing of compressional direction from a ~NNE orientation away from the ATF to a fault-normal orientation near the ATF is consistent with the formation of the observed arc-shaped thrusts (Figure 6a). To balance the decrease in fault-parallel shear (σ_{yz}), stress equilibrium conditions require an increase of basal shear (σ_{xy}) acting on horizontal décollement layers adjacent to the fault (see appendix). Further derivation of the stress equilibrium equation suggests that the width of the arc-shaped thrust faults (L and l in Figure 6a) is related to the depth of thrust décollement (D and d in Figure 6a). A similar pattern is observed in fracture modeling experiments showing that the width of the zone of stress rotation is roughly proportional to the thickness of the fractured layer [*Bai and Pollard*, 2000; *Lawn and Wilshaw*, 1975; *Pollard and Segall*, 1987]. Allowing that these properties are applicable to the ATF, we interpret the tighter curve of the Tula syncline to indicate a shallower décollement within the crust, while the broader arc of the Qimen Tagh thrust system possibly reflects lithospheric scale deformation allowing subduction of Qaidam under Tibet [*Chen and Ozalaybey*, 1998; *Meyer et al.*, 1998; *Tapponnier et al.*, 1990; *Yin and Harrison*, 2000].

Appendix A

[17] We consider the stress equilibrium equation

$$\partial\sigma_{ij}/\partial i + \rho b_j = 0, \tag{A1}$$

where σ_{ij} are the stress components, b_j are body forces per unit volume, and ρ is the density.

[18] In the coordinate system of Figure 6a ($x_1 = x$, $x_2 = y$, $x_3 = z$), we consider a fault of infinite length in the y direction such that derivatives in y are nil and the y term of the equation simplifies to

$$\partial\sigma_{xy}/\partial x + \partial\sigma_{yz}/\partial z = 0. \tag{A2}$$

This expression implies that a decrease of fault-parallel shear (σ_{yz}) is compensated by an increase of basal shear on the décollement layer (σ_{xy}).

[19] Let L be the width of the arcuate structure and D the depth to the décollement. We assume that for a weak ATF, $\sigma_{xy} \sim 0$ at x = 0 (at the fault surface) and increases linearly to $\sigma_{xy} = \sigma^{L}{}_{xy}$ for $x < -L$ (away from the fault). Similarly, we assume linear increase of σ_{yz} from $\sigma_{yz} = 0$ at z = 0 to $\sigma_{zy} = \sigma^{D}{}_{yz}$ at z = D (at the depth to the décollement). The above expression can then be simplified to:

$$-\sigma^{L}_{xy}/L + \sigma^{D}_{yz}/D = 0; \quad \text{(A3)}$$

that is,

$$\sigma^{L}_{xy}/\sigma^{D}_{yz} = L/D. \quad \text{(A4)}$$

The same relationship can be derived for the smaller scale arcuate structure with l (width of arcuate structure) and d (depth to décollement):

$$\sigma^{l}_{xy}/\sigma^{d}_{yz} = l/d. \quad \text{(A5)}$$

Under our linear assumptions, we can express

$$\sigma^{L}_{xy} = \alpha\sigma^{l}_{xy} \quad \text{(A6)}$$

and

$$\sigma^{D}_{yz} = \beta\sigma^{d}_{yz}, \quad \text{(A7)}$$

where α and β are arbitrary constants.

[20] Substituting (6) and (7) into (4) and dividing (4) by (5) yields

$$L/D = l/d.\alpha/\beta \quad \text{(A8)}$$

This last equation indicates the existence of a scaling relationship between the width of the arcuate structure and the depth to the décollement.

[21] **Acknowledgments.** This research was funded by grant EAR 9725663 from the Continental Dynamics Program of the National Science Foundation. Logistical support was provided by Wang Xiao-Feng, Qiao Wan-Song, and Zhang Yue-Qiao at the Institute of Geomechanics, Chinese Academy of Geological Sciences, Beijing, China. We are particularly grateful to Eric Cowgill for introducing us to fieldwork in Xingjiang and to Ramon Arrowsmith for providing the opportunity of a second field season in the Tula area. Laboratory assistance was provided by Bill Hart and Lucas Murray. We thank George Zandt and Pete DeCelles for invaluable discussions. L. J. Sonder, D. Evans, and an anonymous reviewer provided thoughtful reviews.

References

Apotria, T. G., W. T. Snedden, J. H. Spang, and D. V. Wiltschko (1992), Kinematic models of deformation at an oblique ramp, in *Thrust Tectonics*, edited by K. R. McClay, pp. 141–154, Chapman and Hall, New York.

Avouac, J. P., and P. Tapponnier (1993), Kinematic model of active deformation in central Asia, *Geophys. Res. Lett.*, *20*, 895–898.

Bai, T., and D. D. Pollard (2000), Fracture spacing in layered rocks: A new explanation based on the stress transition, *J. Struct. Geol.*, *22*, 43–57.

Bendick, R., R. Bilham, J. Freymueller, K. Larson, and G. Yin (2000), Geodetic evidence for a low slip rate in the Altyn Tagh fault system, *Nature*, *404*, 69–72.

Besse, J., and V. Courtillot (2002), Apparent and true polar wander and the geometry of the geomagnetic field over the last 200 Myr, *J. Geophys. Res.*, *107*(B11), 2300, doi:10.1029/2000JB000050.

Burchfiel, B. C., D. Quidong, P. Molnar, L. Royden, W. Yipeng, Z. Peizhen, and Z. Weiqi (1989), Intracrustal detachment zones of continental deformation, *Geology*, *17*, 448–452.

Chen, W. P., and S. Ozalaybey (1998), Correlation between seismic anisotropy and Bouguer gravity anomalies in Tibet and its implications for lithospheric structures, *Geophys. J. Int.*, *135*, 93–101.

Demarest, H. H. (1983), Error analysis of the determination of tectonic rotations from paleomagnetic data, *J. Geophys. Res.*, *88*, 4321–4328.

Dupont-Nivet, G., R. F. Butler, A. Yin, and X. Chen (2002a), Paleomagnetism indicates no Neogene rotation of the Qaidam Basin in North Tibet during Indo-Asian Collision, *Geology*, *30*, 263–266.

Dupont-Nivet, G., Z. Guo, R. F. Butler, and C. Jia (2002b), Discordant paleomagnetic direction in Miocene rocks from the central Tarim Basin: Evidence for local deformation and inclination shallowing, *Earth Planet. Sci. Lett.*, *199*, 473–482.

Dupont-Nivet, G., R. F. Butler, A. Yin, and X. Chen (2003), Paleomagnetism indicates no Neogene vertical axis rotations of the northeastern Tibetan Plateau, *J. Geophys. Res.*, *108*(B8), 2386, doi:10.1029/2003JB002399.

England, P., and D. McKenzie (1982), A thin viscous sheet model for continental deformation, *Geophys. J. R. Astron. Soc.*, *70*, 295–321.

England, P., and R. E. Wells (1991), Neogene rotations and quasicontinuous deformation of the Pacific Northwest continental margin, *Geology*, *19*, 978–981.

Enkin, R. J., Y. Chen, V. Courtillot, J. Besse, L. Xing, Z. Zhang, Z. Zhuang, and J. Zhang (1991), A Cretaceous pole from south China, and the Mesozoic hairpin turn of the Eurasian apparent polar wander path, *J. Geophys. Res.*, *96*, 4007–4027.

Fisher, R. A. (1953), Dispersion on a sphere, *Proc. R. Soc. London, Ser. A*, *217*, 295–305.

Guo, Z., Z. Zhang, and F. Zeng (1998), Discovery of a mega-thick oil sandstone and asphalt in the Jurassic system in the Tula basin and its significance, *Chin. Sci. Bull.*, *43*, 1898–1901.

Houseman, G., and P. England (1996), A lithospheric-thickening model for the Indo-Asian collision, in *World and Regional Geology Series*, edited by A. Yin and T. M. Harrison, pp. 3–17, Cambridge Univ. Press, New York.

Kirschvink, J. L. (1980), The least-square line and plane and the analysis of paleomagnetic data, *Geophys. J. R. Astron. Soc.*, *62*, 699–718.

Lawn, B. R., and T. R. Wilshaw (1975), *Fracture of Brittle Solids*, Cambridge Univ. Press, New York.

Lockley, M. G., B. D. Ritts, and G. Leonardi (1999), Mammal track assemblages from the Early Tertiary of China, Peru, Europe and North America, *PALAIOS*, *14*, 398–404.

McFadden, P. L. (1990), A new fold test for palaeomagnetic studies, *Geophys. J. Int.*, *103*, 163–169.

McFadden, P. L., and M. W. McElhinny (1990), Classification of the reversal test in palaeomagnetism, *Geophys. J. Int.*, *103*, 725–729.

McKenzie, D., and J. Jackson (1983), The relationship between strain rates, crustal thickening, palaeomagnetism, finite strain and fault movements within a deforming zone, *Earth Planet. Sci. Lett.*, *65*, 182–202.

Meriaux, A., F. J. Ryerson, P. Tapponnier, J. Van der Woerd, R. C. Finkel, M. W. Caffee, C. Lasserre, X. Xu, H. Li, and Z. Xu (2000), Fast extrusion of the Tibet Plateau: A 3cm/yr, 100Kyr slip-rate on the Altyn Tagh fault, *Eos Trans.*, *81*(48), Fall Meet. Suppl., Abstract T62D-07.

Meyer, B., P. Tapponnier, L. Bourjot, F. Metivier, Y. Gaudemer, G. Peltzer, G. Shummin, and C. Zhitai (1998), Crustal thickening in the Gansu-Qinghai, lithospheric mantle, oblique and strike-slip controlled growth of the Tibetan Plateau, *Geophys. J. Int.*, *135*, 1–47.

Molnar, P., and P. Tapponnier (1975), Cenozoic tectonics of Asia: Effects of a continental collision, *Science*, *189*, 419–426.

Molnar, P., B. C. Burchfiel, L. K'uangyi, and Z. Ziyun (1987), Geomorphic evidence for active faulting in the Altyn Tagh and northern Tibet and qualitative estimates of its contribution to the convergence of India and Eurasia, *Geology*, *15*, 249–253.

Nelson, M. R., and C. H. Jones (1987), Paleomagnetism and crustal rotations along a shear zone, Las Vegas Range, southern Nevada, *Tectonics*, *6*, 13–33.

Peltzer, G., and F. Saucier (1996), Present-day kinematics of Asia derived from geologic fault rates, *J. Geophys. Res.*, *101*, 27,943–27,956.

Peltzer, G., P. Tapponnier, and R. Armijo (1989), Magnitude of late Quaternary, left-lateral movement along the north edge of Tibet, *Science*, *246*, 1285–1289.

Pollard, D. D., and P. Segall (1987), Theoretical displacements and stresses near fractures in rocks: With applications to faults, joints, veins, dikes and solution surfaces, in *Fracture Mechanics of Rock*, edited by B. K. Atkinson, pp. 277–349, Academic, San Diego, Calif.

Robinson, D. M., G. Dupont-Nivet, G. E. Gehrels, and Y. Zhang (2002), The Tula uplift, northwestern

China: Evidence for regional tectonism of the northern Tibetan plateau, *Geol. Soc. Am. Bull.*, *115*, 35–47.

Tapponnier, P., G. Peltzer, A. Y. Le Dain, R. Armijo, and P. Cobbold (1982), Propagating extrusion tectonics in Asia: New insights from simple experiments with plasticine, *Geology*, *10*, 611–616.

Tapponnier, P., et al. (1990), Active thrusting and folding in the Qilian Shan, and decoupling between upper crust and mantle in northeastern Tibet, *Earth Planet. Sci. Lett.*, *97*, 382–403.

Washburn, Z., J. R. Arrowsmith, G. Dupont-Nivet, W. X. Feng, Y. Q. Zhang, and Z. Chen (2003), Paleoseismology of the Xorkol segment of the central Altyn Tagh Fault, Xinjiang, China, *Ann. Geofis.*, *46*(5), in press.

Wilkerson, M. S., S. Marshak, and W. Bosworth (1992), Computerized tomographic analysis of displacement trajectories and three-dimensional fold geometry above oblique thrust ramps, *Geology*, *20*, 439–442.

Xinjiang Bureau of Geological and Mineral Resources (XBGRM) (1993), *Regional Geology of the Xinjiang Uygur Autonomous Region: Xinjiang Bureau of Geological and Mineral Resources*, 841 pp., Geol. Publ. House, Beijing.

Yin, A., and M. T. Harrison (2000), Geologic evolution of the Himalayan-Tibetan orogen, *Annu. Rev. Earth Planet. Sci.*, *28*, 211–280.

Yin, A., and S. Y. Nie (1996), Phanerozoic palinspastic reconstruction of China and its neighboring regions, in *Tectonic Evolution of Asia*, vol. IX, edited by A. Yin and T. M. Harrison, pp. 442–485, Cambridge Univ. Press, New York.

Yue, Y., B. D. Ritts, and S. A. Graham (2001), Initiation and long-term slip history of the Altyn Tagh fault, *Int. Geol. Rev.*, *43*, 1087–1093.

Zoback, M. D. (2000), Strength of the San Andreas, *Nature*, *405*, 31–32.

Zoback, M. D., et al. (1987), New evidence on the state of stress of the San Andreas fault system, *Science*, *238*, 1105–1111.

R. F. Butler and H. J. Melosh, Department of Geosciences, University of Arizona, Tucson, Arizona 85721, USA.

G. Dupont-Nivet, Paleomagnetic Laboratory "Fort Hoofddjk," Utrecht University, Budapestlaan 17, NL-3584 CD Utrecht, Netherlands. (gnd@geo.uu.nl)

D. Robinson, Department of Geological Sciences, University of Alabama, 202 Bevill Building, Tuscaloosa, AL 35487, USA. (dmr@wgs.goe.ua.edu)

A. Yin, Department of Earth and Space Sciences, University of California, Los Angeles, California 90095 USA. (yin@ess.ucla.edu)